Scripta Materialia 210 (2022) 114455

Contents lists available at ScienceDirect

Scripta Materialia

journal homepage: www.elsevier.com/locate/scriptamat

TGO formation and oxygen diffusion in Al-rich gamma-TiAl PVD-coatings on TNM alloys

S. Kagerer[a,*], O.E. Hudak[a,b], M. Schloffer[c], H. Riedl[a,b], P.H. Mayrhofer[a]

[a] Institute of Materials Science and Technology, TU Wien, Vienna A-1060, Austria
[b] Christian Doppler Laboratory for Surface Engineering of high-performance Components, TU Wien, Austria
[c] MTU Aero Engines, Muenchen D-80995, Germany

ARTICLE INFO

Article history:
Received 18 August 2021
Revised 27 November 2021
Accepted 29 November 2021

Keywords:
Oxidation resistance
γ-TiAl
TNM
Diffusion coefficients
PVD
Protection coatings

ABSTRACT

γ-TiAl alloys have gained much attention due to their low density, excellent fatigue resistance, and high specific strength at elevated temperatures. Throughout this study, we showcase physical vapor deposited Al-rich γ-TiAl coatings as a considerable solution to extend the durability and longevity of γ-TiAl bulk materials in high temperature regimes (> 750 °C). In detail, the oxidation resistance is enhanced up to at least 850 °C for 1000 h, whilst exhibiting a maximum oxygen affected area of 8.4 µm (16 µm coating). Based on various oxidation treatments (800, 850, and 900 °C), we estimated a mean parabolic rate constant of about $1.03 \bullet 10^{-10}$ cm²/h and a logarithmic oxygen inward diffusion rate of approximately $1.20 \bullet 10^{-4}$ cm/h. The corresponding activation energies validate the considerably retarded oxide scale kinetics – particularly, for the thermally grown oxides. Furthermore, the thermal exposure introduced excellent intermixing between the Al-rich γ-TiAl coating and γ-TiAl bulk material, resulting in a coalescence of the coating-substrate interface.

Innovative materials design and manufacturing has always pioneered technological advancements. This especially holds true in aviation and aeronautic industries, where improved fuel efficiencies and superior engine performances constantly call for lighter and more durable high-temperature materials [1].

Compared to state-of-the-art nickel-based super alloys, intermetallic gamma titanium aluminides (γ-TiAl) show great promise as alternative structural materials, due to their low densities (~4.1 g/cm^3), as well as outstanding fatigue and creep resistance throughout high temperature regimes [2–4]. Especially, the TNM-B1 alloy (Ti-43.5Al–4Nb–1Mo-0.1B at.%) features excellent mechanical properties as wrought alloy [5,6]. However, due to the rather poor oxidation resistance of γ-TiAl-based alloys above 750 °C, the development and tailoring of protective coatings are imperative for their establishment throughout high performance technologies [7]. This has encouraged researchers to develop different thermal barrier coatings (TBCs), such as yttrium stabilized zirconia (YSZ), which decrease the direct influence of the temperature on the protected component across the coating thickness. In order to accommodate the thermal expansion mismatch between the ceramic coating and metal alloy, TBC feature high degrees of porosity. As a consequence, TBC cannot prevent oxygen diffusion and subsequent attack of the substrate surfaces below [8–11]. Therefore, additional oxidation protection coatings are needed. In particular, continuous Al_2O_3-based oxide has emerged as the prominent representative among protective thermally grown oxides (TGO). Unfortunately, the direct deposition of Al_2O_3 onto γ-TiAl-based materials demands for extremely challenging deposition conditions and often bares the disadvantage of thermal mismatches between the protective Al_2O_3 coatings and underlying titanium aluminide substrates [12,13].

Prominent candidates promoting the formation of an Al_2O_3-based TGO are sprayed MCrAlY coatings [14–16]. These have typical thicknesses up to 200 µm, but offer only limited adhesion to the γ-TiAl-based alloys [17–20]. Therefore, the use of PVD grown metallic TiAlCrX (X = Zr, Y) coatings have shown to be extremely beneficial, as they combine excellent oxidation resistance (through the formation of an Al_2O_3-based TGO) with excellent adhesion to γ-TiAl-based (Ti-48Al-2Nb-2Cr) substrate materials [21–23]. However, the diffusion of Cr into the TNM substrate materials leads to a Cr depletion of the TiAlCrX coating, and induces unintended microstructural changes within the TNM substrates [21–23].

A more applicable and elegant solution for improving the oxidation resistance of γ-TiAl-based alloys is provided by a well adherent Al-rich TiAl coating. By incorporating the same elements

* Corresponding author.
E-mail address: stefan.kagerer@tuwien.ac.at (S. Kagerer).

https://doi.org/10.1016/j.scriptamat.2021.114455

from the bulk substrate in the coating, but with a higher Al fraction, a similar thermal expansion coefficient is obtained with a lower probability for delamination due to thermal impact. In this study, a TNM-B1 alloy (Ti-43.5Al–4Nb–1Mo-0.1B at.%) was used as substrate material, to be protected with a physical vapor deposited Al-rich TiAl coating (using a [Ti-62Al-4Nb-1Mo-0.3(B+Y)] target material [24,25]). The effectiveness of this concept depends on various diffusion related mechanisms: (i) The development of the Al_2O_3-based TGO including the Al outward diffusion, (ii) the inward diffusion of oxygen (representing how effective this TGO can reduce the oxygen inward diffusion into the coating), and (iii) the Al inter-diffusion from the Al-rich TiAl coating into the γ-TiAl-based (TNM bulk material) substrate material. The latter results in Al-depleted regions within the coating, and contrarily Al-enriched regions within the γ-TiAl-based substrate. We want to emphasize, that the Al-depleted region within the coating still contains more Al than the Al-enriched regions of the substrate. For protective coatings, the depletion of elements through diffusion into the bulk material (*e.g.*, TNM alloys), will eventually have negative consequences for their lifetime and performance. This is especially important when considering Al, which influences the nature of the Al_2O_3-based.

TGO. With the objective to better understand the diffusion processes at hand and allow predictions about the lifetime of the protective coating well beyond laboratory data, two diffusion processes were studied in detail: (i) The oxidation of the coating surface (including the formation of an Al_2O_3-based TGO and the oxygen inward diffusion), and (ii) the corresponding influence of Al inter-diffusion between the coating and γ-TiAl-based substrate. Although, it is always the gradient in chemical potential that drives diffusion, the phenomenological description by Fick (Fickś first and second law of diffusion and the resulting "Einstein-Smoluchowski-relation" through the chemical gradient) are simple and efficient tools for calculating the respective parabolic rate constant (k_p), the parabolic rate preexponential factor (k_{p0}), and activation energies (q). Together, these values allow for an estimation of the lifetime and performance of the coating [26–29].

For means of increasing the oxidation resistance of industrially established γ-TiAl-based TNM alloys, Al-rich TiAl coatings with ~6, 12, and 16 µm thickness were deposited by non-reactive unbalanced magnetron sputtering using a [Ti-62Al-4Nb-1Mo-0.3(B+Y)] target (6-inch cathode) [24]. A deposition rate of 55 nm/min was achieved by applying 4.5 W/cm² to the target. In a pre-step the substrates were electrochemically polished (Struers A3 electrolyte) and subsequently cleaned, as well as degreased (sodium-hydroxide

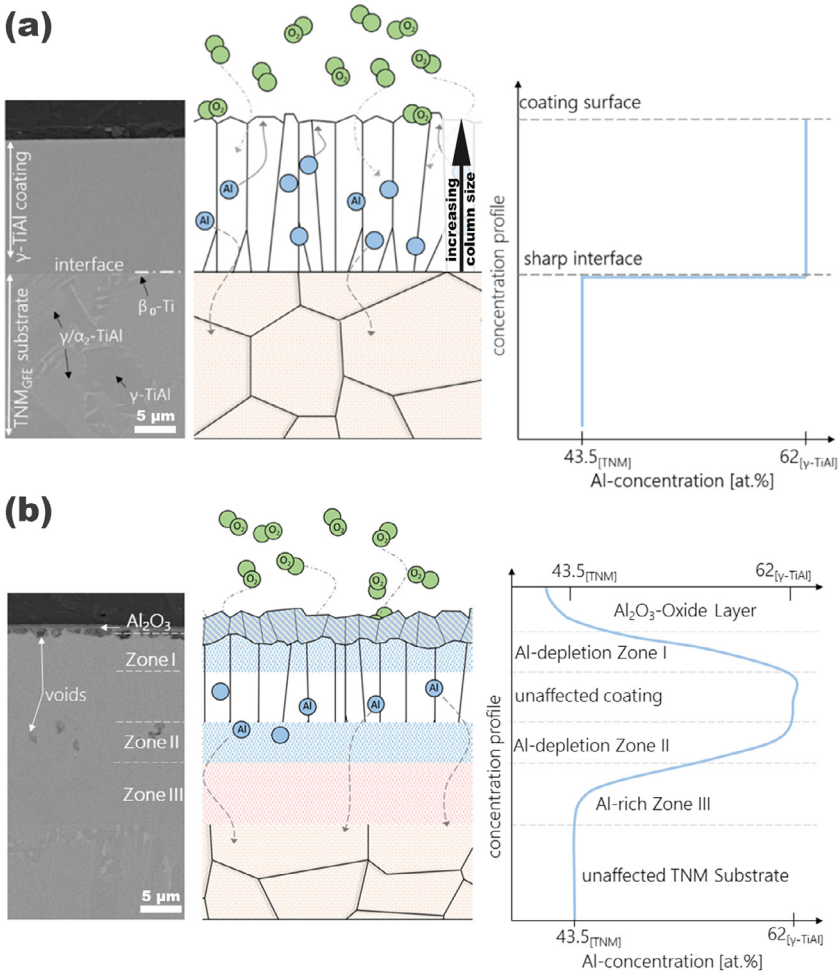

Fig. 1. Cross-section BSE-SEM images and corresponding schematic illustrations highlighting the predominant O- and Al-diffusion paths of the 16-µm-thick Al-rich TiAl-based coating on the TNM substrate in the as-deposited state (a) and after oxidation for 100 h at 900 °C (b). The EDS-obtained Al line profiles highlight the Al_2O_3 formation, the still present Al-reservoir (where the TiAl-based coating still shows its original Al content, named as unaffected coatings in (b)), and the coating/substrate interdiffusion due to this thermal treatment. In combination with the BSE-SEM image, the Al line profile allowed to identify the following regions as well: Aldepletion zone I directly underneath the oxide (dotted blue region in the schema), Al-depletion zone II immediately above the interface to the substrate (dotted blue region in the schema), and an Al-rich zone III immediately below the original interface to the coating (dotted red region in the schema).

and 2-aminoethanol solution). In addition, the substrates were rinsed with distilled water and cleaned in an ultrasonic bath for 10 min. All depositions were conducted with an "in-house" developed semi-industrial scaled unbalanced magnetron sputtering system [30]. The pre-cleaned substrates were mounted onto a rotating substrate holder (90 rad/s) within the deposition chamber and subsequently heated to $T_{sub} \leq 300$ °C. This low deposition temperature beware the TNM of getter small amounts of oxygen which causes an embrittlement of the TNM during the substrate heating. Additional temperature induced microstructural changes can be excluded and highlights the excellent capabilities of PVD based techniques compared to other deposition routes *e.g.* thermal spraying.

After maintaining the temperature for 20 min, the samples were ion-etched with Argon (p_{etch}= 6 Pa) for 10 min by biasing the substrates with U_{bias}= -500 V. For the actual deposition an Ar gas pressure of p_{dep}= 0.4 Pa was maintained. In addition, a bias potential of U_{bias}= -50 V was applied [24].

To investigate the cross-sectional morphology of the coatings, back scattered electron (BSE) scanning electron microscopy (SEM) with a FEI Quanta 200 FEG-SEM and a 10 kV acceleration voltage was used. Fig. 1a shows an image of a 16 µm thick Al-rich γ-TiAl-based coating in its as-deposited state on the TNM substrate. The Al-rich coating is predominantly γ-TiAl structured ($L1_0$ crystal structure) and features a homogenous contrast during this stage of the investigation. Contrary, the TNM substrate shows a homogenous distribution of α_2/γ-TiAl grains ($D0_{19}/L1_0$-crystall structures) and γ-TiAl grains surrounded by β_0-grains at the colony boundaries [31]. Due to these differences in phase-contrast, the interface between coating and TNM substrate is clearly visible.

The difference in microstructure between coating and TNM bulk alloy is also schematically given in Fig. 1a. The coating exhibits columnar grains with significantly smaller sizes (in average the columns are 200 nm long and 50 nm wide, as obtained from detailed SEM and XRD investigations) than the large α_2/γ grains of the TNM bulk (more than 5 µm). Fig. 1a also shows the initially sharp gradient of aluminum between coating (62 at.% Al) and TNM substrate (43.5 at.% Al).

The microstructural changes due to thermal exposure after 100 h at 900 °C in ambient air are presented in Fig. 1b. The oxygen diffusion and reaction with the coating material leads to the formation of an alumina-based scale. Accordingly, the γ-TiAl coating is depleted of Al directly underneath the TGO, which is denoted as Al-depleted zone I in Fig. 1b. Simultaneously, interdiffusion processes between coating and TNM substrate lead to the smoothening of the sharp Al-concentration gradient. This causes the formation of a second Al-depletion zone within the coating and an Al-enriched zone in the underlying TNM substrate, marked as Al depleted zone II and Al-rich zone III, respectively (Fig. 1b). Due to the increased Al content in the coating-near substrate region, the original TNM microstructure transforms towards a homogeneous appearance in the BSE-SEM image (Fig. 1b). This is also highlighted in the schematic cross-section next to this image. The interdiffusion between TNM substrate and Al rich γ-TiAl-based coating leads to an outstanding adhesion. The Kirkendall voids that develop within the coating, directly underneath the Al_2O_3-based TGO and close to the TNM substrate (zone II), are a clear sign for an accelerated outward-diffusion of Al, leaving vacancies in these regions that further condense to voids. The concentration gradient along the entire cross section (Fig. 1b) coincides perfectly with the microstructural transformation observed during BSE-SEM, and allowed to adequately represent the processes in the schematic sketch. Clearly, a region with the original high Al content of 62 at.% is still present after 100 h at 900 °C in this 16 µm-thick PVD coating.

To quantify the oxidation kinetics, the γ-TiAl coated materials were oxidized at 800, 850 and 900 °C for 1, 10, 30, and 100 h, and subsequently investigated in detail using EDX line-scans. In order

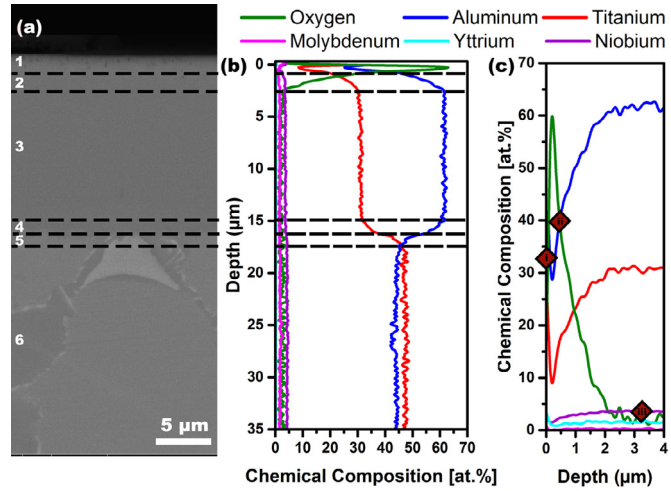

Fig. 2. (a) Cross-sectional BSE-SEM image of the originally 16-µm-thick Al-rich TiAl-based coating on a TNM substrate after 30 h oxidation treatment at 850 °C. (b) Corresponding EDS line scan with the y-axis aligned to the BSE-SEM image. (c) Detailed view of the EDS line scans outer most 4 µm. The marked points (i: O exceeds Al; ii: Al exceeds O; iii: O signal reaches the as-received value within the TNM alloy) were used to obtain the TGO thickness, x_{TGO}, and the oxygen inward diffusion zone underneath the TGO, x_{Ox}, using Eqs. (1) and (2).

to profile chemical changes, an EDAX SDD Octane Elite 55 detector with 20 kV accelerating voltage was utilized. An exemplary BSE-SEM image and characteristic line scan after 30 h at 850 °C is presented in Fig. 2a and b, respectively. The changes in microstructure (Fig. 2a), due to the different Al-content (Fig. 2b) within the coating and TNM substrate, and also the oxide scale formation with an accompanied oxygen inward diffusion is clearly visible. The interdiffusion between the coating (Al-depletion zone II) and the TNM bulk material (Al rich zone III) leads to a structural interfacial homogenization, and results in the already mentioned outstanding coating to substrate adhesion.

As defined above, the various zones with different Al-contents are named according to their change from the as-deposited condition. The Al-depleted zone II lies within the original coating region (but close to the TNM substrate) and the Al-rich zone III exists within the original substrate region (but close to the coating). Although zone II is termed Al depleted zone, it still retains a higher Al content than zone III, which is named Al-rich. As illustrated in Fig. 2c, we identified three different specific diffusion distances, indicated by (i) where oxygen exceeds the Al at.% content, (ii) where Al- exceeds the oxygen content, and (iii) where the oxygen signal approaches the oxygen content of the bulk material in its as-received state. Respectively, (i), (ii), and (iii), as shown in the line-scan (Fig. 2c), have been used for evaluating the respective oxide growth thickness (x_{TGO}) and oxygen inward diffusion depth (x_{Ox}) according to:

$$x_{TGO} = x_{ii} - x_i \tag{1}$$

$$x_{Ox} = x_{iii} - x_{ii} \tag{2}$$

The growth kinetics of the TGO can best be described with a parabolic rate law, see Eq. (3), where t is time. On the contrary, the profile of the oxygen inward diffusion best matches a logarithmic function, Eq. (4). An explanation for the two different rate-law can be provided by considering that the oxygen for this inward diffusion is basically provided by/through the TGO.

$$x_{TGO} = \sqrt{k_p \cdot t} \tag{3}$$

$$x_{Ox} = d_{Ox} \cdot \log(t) \tag{4}$$

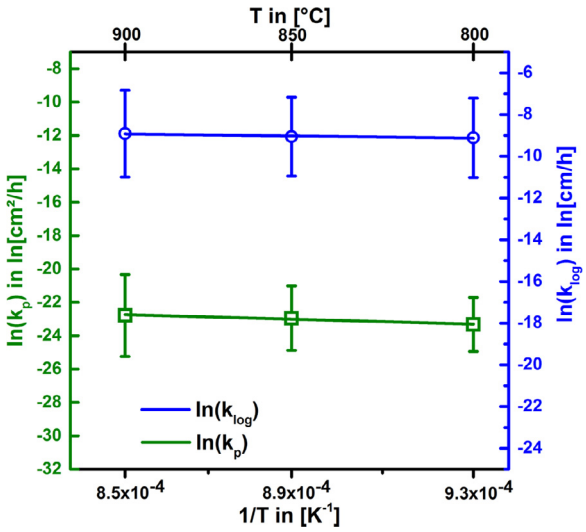

Fig. 3. Arrhenius plots of the k_p values obtained for the TGO growth and the d_{ox} values obtained for the oxygen inward diffusion zone underneath the TGO (Table 1). The empty green symbols and the corresponding linear fit represent the TGO formation and the blue empty circles and the corresponding linear fit show the oxygen inward diffusion. The error bars of the individual data stem from the investigation of three samples per oxidation treatment step.

Table 1
The mean parabolic rate constants for the TGO growth and the mean logarithmic inward diffusion rates for 800, 850 and 900 °C.

T_{Ox} (°C)	k_p (cm²/h) TGO	d_{Ox} (cm/h)
800	$7.40\cdot10^{-11} \pm 1.4\cdot10^{-11}$	$1.10\cdot10^{-4} \pm 1.65\cdot10^{-5}$
850	$1.08\cdot10^{-10} \pm 1.57\cdot10^{-11}$	$1.17\cdot10^{-4} \pm 1.77\cdot10^{-5}$
900	$1.26\cdot10^{-10} \pm 1.08\cdot10^{-11}$	$1.35\cdot10^{-4} \pm 1.69\cdot10^{-5}$

With increasing oxidation time and temperature, the thermally grown oxide clearly thickens.

Despite different thicknesses of the γ-TiAl based coatings (~6, 12, and 16 µm), roughly the same TGO scale thicknesses of ~0.6 to ~1.2 µm were obtained after isothermal annealing for 100 h at 800, 850 and 900 °C.

Table 1 contains the parabolic rate constants for the TGO, averaged from three samples per oxidation treatment of 1, 10, 30, and 100 h at 800, 850, and 900 °C. Furthermore, the mean logarithmic inward diffusion rates for the oxygen inward diffusion underneath the TGO are also obtained from the average values of the samples per treatment of 1, 10, 30, and 100 h at 800, 850, and 900 °C.

The activation energies for the TGO formation (q_{kp}) and the oxygen inward diffusion (q_{Ox}) are obtained from Arrhenius plots, Fig. 3, of Eqs. (5) and (6) [28,32–34] – with k_B being the Boltzmann's constant – using the mean values obtained for 800, 850, and 900 °C presented in Table 1.

$$k_p = k_{p0} \cdot e^{-\frac{q_{kp}}{k_B T}} \tag{5}$$

$$d_{Ox} = d_{Ox0} \cdot e^{-\frac{q_{Ox}}{k_B T}} \tag{6}$$

The intercepts of the linear fits with the ordinate of the Arrhenius plots provide the pre-exponential factors, k_{p0} and d_{Ox0}, while the slope provides the activation energies, q_{kp} and q_{Ox}, for these processes. Thus, the pre-exponential factor for the oxygen inward diffusion is d_{Ox0} =

0.00114 cm/h, while the pre-exponential factor for the TGO growth is k_{p0}= $5.67\cdot10^{-8}$ cm²/h. The activation energy for the TGO formation (q_{kp}= 0.61 eV) is much larger than that for the oxygen inward diffusion (q_{Ox}= 0.22 eV). The latter is in excellent agreement with literature values [35], where an energy barrier for oxygen diffusion from the TiAl surface into subsurface layers of 0.28–0.32 eV is reported. The slightly lower activation energy during our experiments suggests for an easier diffusion mechanism in the PVD coating (with their typically high defect density) than in the TiAl alloy.

This data is used to predict the TGO thickness (x_{TGO}) and the oxygen inward diffusion zone (x_{Ox}) up to 1200 h at 850 °C. Fig. 4a shows the combined oxygen affected zone (x_{TGO}+x_{Ox}), whereas Fig. 4b presents the oxygen inward diffusion zone (x_{Ox}). The dashed line is obtained from the mean values at 850 °C (Table 1) and the greyish region is obtained when including the value for the 6 and 16 µm thick coating. To experimentally verify these predictions, γ-TiAl coatings were redeposited (again with ~6, 12, and 16 µm) and oxidized for 100, 600, and 1000 h at 850 °C. Hereafter, the samples were investigated and analyzed according to the previously outlined procedure – see the hollow symbols in Fig. 4a and

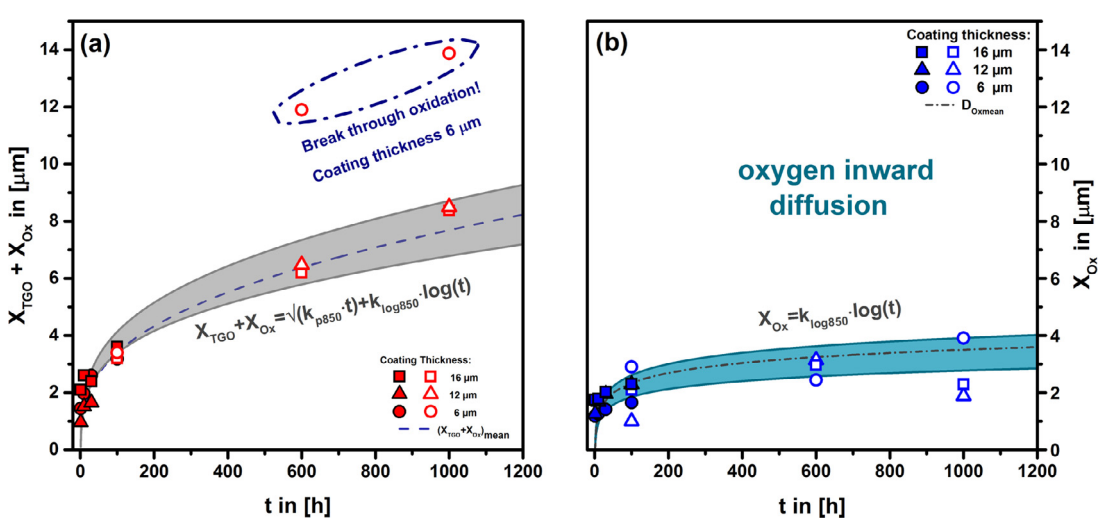

Fig. 4. (a) Time-dependent thickness of the oxygen affected surface near region (combining the TGO thickness, x_{TGO}, and the depth of the oxygen inward diffusion depth, x_{Ox}) during oxidation at 850 °C. (b) Time-dependent oxygen inward diffusion depth, x_{Ox}, underneath the TGO. The solid data points are from samples used to obtain the relevant parameters for the predicted TGO thickness and oxygen diffusion zone depth. Based on these, coatings with the same thicknesses (6, 12, 16 µm) were redeposited on a TNM substrate and investigated as well (empty symbols).

b. The filled symbols represent the data mentioned above, which have been used to obtain the oxygen growth rate and diffusion constants (Table 1), as well as the activation energies to draw the extrapolated lines.

Solely the 6 µm-thin γ-TiAl based coating is too thin for the 850 °C treatment, when exposed for more than 100 h, and exhibits a much thicker oxygen influenced zone than predicted. The depleted Al-reservoir (due to the thin Al-rich TiAl-based coating) causes almost a breakthrough oxidation (clearly visible in SEM). Otherwise, the experimentally obtained data from the thicker γ-TiAl-based coatings accurately correlates with the values from the prediction. By comparing the calculated oxygen inward diffusion depth underneath the TGO (Fig. 4b) – also considering the affected area for the thinnest and thickest coating (blueish area) – with the experimentally obtained data, actually feature a more constant oxygen inward diffusion depth, especially for longer times. This suggests that the TGO formed, is very effective in limiting further oxygen diffusion. The 11 and 16 µm Al-rich TiAl-based coatings allowed for a reduced TGO thickness (3.3–3.7 µm at 600 h) even up to 1000 h (4.5–5.2 µm), with $k_p = 1.08 \bullet 10^{-10}$ cm^2/h and an activation energy of 0.61 eV. Only, if there is an insufficient Al-reservoir to form a continuous and protective Al_2O_3 layer (as it is the case for the 6 µm-thin TiAl-based coating after 600 h and more), the oxygen inward diffusion depth increases. As soon as the Al rich TiAl-based coating is consumed or its Al-content falls below 50 at.%, competing TiO_2 rich regions form within the TGO and lead to spallation of the protective oxide, as well as breakthrough oxidation.

Based on these findings, we conclude that Al-rich γ-TiAl based PVD coatings are well suited as an oxidation protection aid for common TNM-bulk alloys. They allow for the formation of a superior protective TGO, capable of significantly limiting the oxygen inward diffusion depth. Moreover, the very close match in material characteristics, combined with a coalescence of the Al-rich TiAl based coating and TNM substrate interface provides excellent adhesion properties This allows a minimum coating thickness approximation of 9 µm for an isothermal long-term use at 850 °C for at least 1200 h.

Declaration of Competing Interest

The authors declare that they have no known competing financial interests or personal relationships that could have appeared to influence the work reported in this paper.

Acknowledgement

We want to thank MTU Aero Engines AG for the financial support. In addition, we also want to thank the X-ray center (XRC) of TU Wien for beam time as well as the electron microscopy center - USTEM TU Wien - for using the SEM facilities. The financial support by the Austrian Federal Ministry for Digital and Economic Affairs, the National Foundation for Research, Technology and Development and the Christian Doppler Research Association is gratefully acknowledged (Christian Doppler Laboratory "Surface Engineering of high-performance Components"). The authors acknowledge TU Wien Bibliothek for financial support through its Open Access Funding Programme."

References

[1] D.M. Dimiduk, Mater. Sci. Eng. A 263 (1999) 281–288.
[2] M. Burtscher, T. Klein, S. Mayer, H. Clemens, F.D. Fischer, Intermetallics 114 (2019) 106611.
[3] H. Clemens, W. Smarsly, Adv. Mater. Res. 278 (2011) 551–556.
[4] H. Clemens, S. Mayer, Mater. Sci. Forum 879 (2017) 113–118.
[5] M.C. Galetz, A.S. Ulrich, C. Oskay, D. Fähsing, N. Laska, U. Schulz, M. Schütze, Intermetallics 123 (2020) 1–7.
[6] B.P. Bewlay, S. Nag, A. Suzuki, M.J. Weimer, Mater. High Temp. 33 (2016) 549–559.
[7] R. Pflumm, S. Friedle, M. Schütze, Intermetallics 56 (2015) 1–14.
[8] R. Braun, U. Schulz, C. Leyens, P.E. Hovsepian, A.P. Ehiasarian, Int. J. Mat. Res. 101 (2010).
[9] N. Laska, R. Braun, Oxid Met 81 (2014) 83–93.
[10] S. Friedle, N. Nießen, R. Braun, M. Schütze, Surf. Coat. Technol. 212 (2012) 72–78.
[11] R. Braun, C. Leyens, M. Fröhlich, Mater. Corros. 56 (2005) 930–936.
[12] Z. Tang, F. Wang, W. Wu, Materials Science and Engineering A276 (2000) 70–75.
[13] R. Braun, A. Lange, P.E. Hovsepian, A.P. Ehiasarian, R. Tietema, C. Leyens, Materials at High Temperatures 28 (4) (2014) 324–335.
[14] J.D. Béguin, J. Alexis, D. Adian, S. Metayer, T. Masri, J.A. Petit, P. Belaygue, in: Proceedings of the 10th World Conference on Titanium, 2003, pp. 2455–2462. Held CCH-Congress CentHamburg, Ger. July 13-182004.
[15] D.J. Kim, X. Huang, D.Y. Seo, Y.W. Kim, Oxid. Met. 78 (2012) 31–50.
[16] W.G. Sloof, T.J. Nijdam, Int. J. Mater. Res. 100 (2009) 1318–1330.
[17] F.J. Belzunce, V. Higuera, S. Poveda, A. Carriles, J. Therm. Spray Technol. 11 (2002) 461–467.
[18] R. Chen, X. Gong, Y. Wang, G. Qin, N. Zhang, Y. Su, H. Ding, J. Guo, H. Fu, Corros. Sci. 136 (2018) 244–254.
[19] J. Matějíček, M. Vilémová, R. Mušálek, P. Sachr, J. Horník, Coatings 3 (2013) 108–125.
[20] T.N. Rhys-Jones, Surf. Coat. Technol. 42 (1990) 1–11.
[21] N. Laska, R. Braun, S. Knittel, Surf. Coat. Technol 349 (2018) 347–356.
[22] R. Braun, K. Kelm, M. Fröhlich, C. Leyens, Surf. Coat. Technol. 222 (2013) 128–134.
[23] C. Eilers, N. Laska, R. Braun, Surf. Coat. Technol. 223 (2013) 24–31.
[24] M. Schloffer, H. Warnecke, Pub. No.: US 2018/163291 A1, 2018.
[25] W. Smarsly, M. Schloffer, H. Clemens, S. Mayer, Patent No.: US10465264B2, 2019.
[26] A. Fick, Ann. Phys. 170 (1855) 59–86.
[27] A. Einstein, Dover Publications INC. (1956).
[28] M. Smoulchowski, Zeitschrift Für Chemie Und Ind. Der Kolloide 1 (1907) 308–309.
[29] J. Philibert, One and a Half Century of Diffusion: Fick, Einstein, before and beyond, Diffus. Fundam. 2 (2005) 1.1–1.10.
[30] L. Zauner, P. Ertelthaler, T. Wojcik, H. Bolvardi, S. Kolozsvári, P.H. Mayrhofer, H. Riedl, Surf. Coat. Technol. 382 (2020) 125007.
[31] H. Clemens, W. Wallgram, S. Kremmer, V. Güther, A. Otto, A. Bartels, Adv. Eng. Mater. 10 (2008) 707–713.
[32] A. Einstein, Ann. Phys. 322 (1905) 549–560.
[33] C. Sabitzer, C. Steinkellner, C.M. Koller, P. Polcik, R. Rachbauer, P.H. Mayrhofer, Surf. Coat. Technol. 275 (2015) 185–192.
[34] E. Aschauer, T. Wojcik, P. Polcik, O. Hunold, M. Arndt, V. Dalbauer, P.H. Mayrhofer, P. Felfer, H. Riedl, Mater. Des. 201 (2021) 109499.
[35] A.V. Bakulin, S.E. Kulkova, Q.M. Hu, R. Yang, J. Exp. Theor. Phys. 120 (2015) 257–267.